Experimental proof of standard electrodynamics by measuring the self-force on a part of a current loop

G. Cavalleri,* G. Bettoni, and E. Tonni*
Dipartimento di Matematica e Fisica, Università Cattolica del Sacro Cuore, via Trieste 17, 25121 Brescia, Italy

G. Spavieri†
Centro de Astrofísica Téorica, Universidad de Los Andes, Mèrida 5101, Venezuela
(Received 15 December 1997)

The results of measurements of the force on a part of a circuit carrying a steady current, due to the action of the whole current loop, are reported. The theoretical value of the force has been calculated using the standard electrodynamics force law. Taking into account the finite dimension of the wire forming the current loop, the calculation implies the computation of a sixfold integral. Contrary to the past experimental outcome reported in the literature, a comparison of a theoretical predictions with the present experimental results corroborates the standard force law within the limits of experimental errors. [S1063-651X(98)11706-3]

PACS number(s): 41.20.Jb, 41.90.+e, 03.30.+p

I. INTRODUCTION

In this paper we present the experimental results and the relevant theory regarding the electromagnetic force due to the electric current flowing in a closed circuit and acting on a part of it. The experiment performed is like that of Ampère. However, a comparison of theory and experiment could not be done before the advent of modern computers. Indeed, the self-force **F** (of a part of a circuit on itself) cannot be calculated in the approximation of an ideal wire with zero cross section carrying a steady current because **F** would diverge logarithmically when the radius a of the wire tends to zero. **F** has to be calculated as the integral over all the volumes, i.e., by a sixfold integral.

Before discussing the experiment, it is important to clarify a point we did not find in the literature. It is often written that what we measure are forces between closed circuits and we can draw from them infinite different elementary laws that express the forces between two elements of the wires. The most famous expressions are those of Grassmann (sometimes called the *Biot-Savart law*) and Ampère [1]. Some of us [1] have shown that the Ampère and Biot-Savart elementary laws lead to the same result even for the force on a part of a circuit and due to the whole circuit. However, it is also possible to derive the correct elementary law by considering each element of a wire as composed of several charges at rest (ions) and other opposite charges (electrons) with an average velocity **v**. Then, by applying the Lienard-Wiechert law [valid for a pointlike charge q with any value of its advanced (with respect to the field point at time t) position $\mathbf{r}-\mathbf{r}'$, advanced velocity $\mathbf{v}(t-|\mathbf{r}-\mathbf{r}'|/c)$, and advanced acceleration $\mathbf{a}(t-|\mathbf{r}-\mathbf{r}'|/c)$], we obtain

$$d\mathbf{B}=\frac{\mu_0 dq}{4\pi|\mathbf{r}-\mathbf{r}'|^3\left(1-\frac{\mathbf{v}}{c}\cdot\frac{\mathbf{r}-\mathbf{r}'}{|\mathbf{r}-\mathbf{r}'|}\right)^3}\left\{\mathbf{v}\times(\mathbf{r}-\mathbf{r}')\left(1-\frac{v^2}{c^2}\right)+\frac{\mathbf{a}}{c}\cdot(\mathbf{r}-\mathbf{r}')\mathbf{v}\times\frac{\mathbf{r}-\mathbf{r}'}{c}+\mathbf{a}\times\frac{\mathbf{r}-\mathbf{r}'}{c}\left[|\mathbf{r}-\mathbf{r}'|-\mathbf{v}\cdot\frac{\mathbf{r}-\mathbf{r}'}{c}\right]\right\}. \quad (1)$$

The Laplace expression $d\mathbf{B}=(\mu_0/4\pi)dq\,\mathbf{v}\times(\mathbf{r}-\mathbf{r}')|\mathbf{r}-\mathbf{r}'|^{-3}$ (which leads to the Biot-Savart law) is an approximation to Eq. (1) for $v/c\to 0$ and for negligible acceleration **a**. On the contrary, Ampère's law [given by Eq. (1) of Ref. [1]] is not even an approximation. However, the Lienard-Wiechert expressions and those of Laplace (Biot-Savart) and Ampère give the same result when integrated over a closed circuit.

A stimulus to perform the present experiment came from two rather recent experimental works [2,3] where a disagreement between standard theory and experiments is claimed. Examining Ref. [2], we concluded that the relevant experiment was unreliable for two reasons: the existence of sharp angles, which imply a strong force not considered by Pappas [2], and the use of pulsed currents whose durations depend on the manual technique of the experimenter.

The second experiment [3] is affected by the strong force, comparable to the useful one on the rest of the circuit, due to the electrical connection, and not considered by Phipps [3]. In fact, if the current is the same, the force is the same for circuits of different sizes but similar in shape. Since the two electrical connections used by Phipps [3] are just similar to the main circuit, the total force is three times that acting on the main circuit.

In our experiment we tried to shape the electrical connections so as to be as near as possible to straight lines. Yet the calculations of the forces due to the connections yield about 6% of the total force and they must therefore be considered.

*Electronic address: cavaller@dmf.bs.unicatt.it
†Electronic address: spavieri@ciens.ula.ve

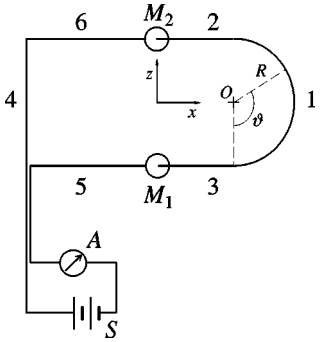

FIG. 1. Sketch of the electrical circuit. The segments 1–6 constituting the circuit are divided into two parts: 1–3 represent the mobile part (on which the force has to be measured) and 4–6 represent the fixed part. R denotes the radius of arc 1 and M_1 and M_2 the two mercury troughs.

The structure of our paper is the following. In Sec. II we describe the electric circuit and the experimental apparatus used to measure the force on a mobile part of the circuit and due to the whole circuit. The mobile part is electrically connected to the fixed part by a mercury trough. In Sec. III we calculate the forces using the mentioned standard theory (the Biot-Savart law). In addition to the difficulty regarding the calculation of a convergent sixfold integral with a divergent integrand, another difficulty consists in calculating the force on the conductor immersed in the mercury trough since, for this task, one has to find the distribution of the currents in the mercury and in the bronze of the trough. Appendix A is dedicated to these long calculations. In Sec. IV we report on the experimental results and agreement with the theoretical predictions. We conclude in Sec. V.

II. EXPERIMENTAL APPARATUS

In order to measure the force acting on a part of the circuit and due to the whole current loop, the part in consideration must be electrically connected to the remaining part but must be free to move with minimum friction with respect to the fixed part. After several attempts, we have found it best to use the traditional method of the mercury trough, as shown in Fig. 1. Moreover, in order to know the current behavior in the parts (1–3) of the circuit on which the force is measured, we have to avoid sharp edges. The mercury troughs M_1 and M_2 provide the electrical connection of the mobile to the fixed part. Three other sections of the circuit are also shown in Fig. 1 (4–6), which represent the fixed part of the circuit (while sections 1–3 represent, as said, the mobile part). With this splitting we can more conveniently calculate the contribution of each section to the **B** field and therefore to the force on each section. In order to calculate the force on parts 1–3, the fixed parts 4–6 may be considered as made of a thin wire while the contribution due to the edges is of little importance. The mobile parts 1–3 must have no edges because on them acts also the force due to the field $\mathbf{B}_m$ produced by the mobile part itself, which requires, for its determination, the computation of a sixfold integral.

The experimental apparatus schematized in Fig. 2 is composed of three systems. The first system, a current supply S plus a digital multimeter A, is used for the generation, the inversion, and measurements of the current. The second system is a variable geometry circuit of the type shown in Fig. 1. The third system allows the measurement of the forces acting on the mobile part by reacting mechanically to any displacement.

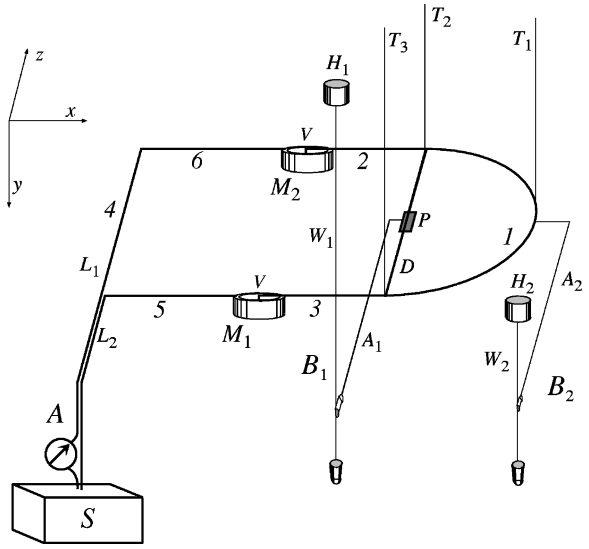

FIG. 2. Sketch of the experimental apparatus. A current supply S feeds a current I_0, measured by an amperometer A (more precisely a multimeter), to the circuit, already schematized in Fig. 1, and supported by three suspension threads T_1, T_2, and T_3. A torsion balance B_1, consisting of a torsion wire W_1 and a torsion angle lecture head H_1, measures the force F acting on the mobile part of the circuit by an arm A_1 connected to the plate P fixed to the insulating rod D. A second torsion balance B_2 (lecture head H_2, wire W_2, and arm B_2) is used to eliminate the mechanical plays. The electrodes V are partially immersed in the mercury contained in the troughs.

The mobile part of the circuit is made of a semicircular arc 1 continuing with two straight segments 2 and 3, at the ends of which there are two electrodes V (see Fig. 2 and, for details, Fig. 5 of Appendix A, where the mercury trough is extensively studied). These electrodes have the purpose, once put in the mercury troughs M_2 and M_1 respectively, of providing the electric contact with the fixed part. The arc is kept rigid by the insulating rod D fixed to it. A rectangular plate P related to the third system is attached to the center of the rod D. The arc is suspended by three threads T_1, T_2, and T_3. The threads T_2 and T_3 are fixed to the ends of the rod D and T_1 is fixed to the middle point of arc 1.

The fixed part has two different possible configurations, one called short ($\mathcal{S}$) and the other long ($\mathcal{L}$). The short one has segments 5 and 6 of negligible length, i.e., $l_5=l_6=0$, while in the long configuration the length of these sections is $l_5=l_6=60.10$ cm. The two mercury troughs M_1 and M_2 belong to the fixed part and, to calculate the force on the distant arc 1, we may approximate M_1 and M_2 to two sections of length equal to their internal radius $r_0=1.52$ cm in the $\mathcal{L}$ configuration since wires 5 and 6 end at the internal lateral surface of the mercury troughs (for details see Fig. 5). In the $\mathcal{S}$ configuration wire 4 is soldered on M_2 so the symmetry axis of wire 4 is a distance $d=0.488$ cm from the internal surface of mercury trough. The same connection occurs for wire 5 that, in the $\mathcal{S}$ configuration, is parallel to wire 4 and separated from it by a thin insulator. The equivalent

lengths of the fixed part in the two configurations are therefore

$$\mathcal{S}:\ l_4=29.10\ \text{cm},$$
$$l_{5\text{eq}}=l_{6\text{eq}}=l=r_0+d=(1.52+0.488)\ \text{cm}=2.008\ \text{cm};$$
$$\mathcal{L}:\ l_4=29.10\ \text{cm},$$
$$l_{5\text{eq}}=l_{6\text{eq}}=l=l_5+r_0=(60.10+1.52)\ \text{cm}=61.62\ \text{cm}. \tag{2}$$

This approximation is not acceptable for the calculation of the force F_V on the section V (see Fig. 2) immersed in the mercury and Appendix A is dedicated to the correct calculation of F_V. Obviously, side 4 is not directly connected to side 5, but both of them are connected to the current supply S, as shown in Figs. 1 and 2. The two connections are very close to each other so that the residual magnetic field produced by them on arc 1 is negligible.

The values of the different sections of the mobile part are the same in both the $\mathcal{L}$ and $\mathcal{S}$ configurations. They are

$$a=0.25\ \text{cm (the radius of all the wires)},$$
$$R=l_4/2=14.55\ \text{cm},\quad l_2=l_3=h=25.45\ \text{cm}. \tag{3}$$

The third system is composed of two parts, one determining the relative position and the other measuring the force acting on the mobile circuit. The part that determines the relative position consists of two electronic barriers, two impulse counters, and the plate P fixed to the middle point of the insulating rod D. The part of the third system that measures the forces acting on the mobile circuit is formed by two torsion balances B_1 and B_2. The second balance B_2 does not intervene directly in the measurements because it has the function of opposing the first one when, in the absence of current, we look for the equilibrium position of the mobile part. Moreover, it has the useful purpose of eliminating the mechanical plays. The displacements of the mobile parts 1–3 are revealed by the interruption of the beam of light emitted by photodiodes on the electronic barriers at the position of the plate P and measured by the impulse counters. When the action of the current displaces the mobile part from the equilibrium position, we shift it back to the original position by rotating the head H_1 of the first balance. In this situation the electromagnetic force is equilibrated by the elastic torsion force of the wire W_1 and the value of the force may be measured.

III. CALCULATION OF THE FORCES ON THE DIFFERENT PARTS OF THE CIRCUIT

As said in the Introduction, Eq. (1) reduces to Laplace's first law when $v/c\to 0$ and the acceleration term is negligible. Since $dq\mathbf{v}=\mathbf{j}d^3r$, we have Laplace's first formula

$$\mathbf{B}(\mathbf{r})=\frac{\mu_0}{4\pi}\int\int\int_{1+2+3+4+5+6} d^3r'\,\mathbf{j}(\mathbf{r}')\times\frac{\mathbf{r}-\mathbf{r}'}{|\mathbf{r}-\mathbf{r}'|^3}. \tag{4}$$

The forces are then calculated by Laplace's second law

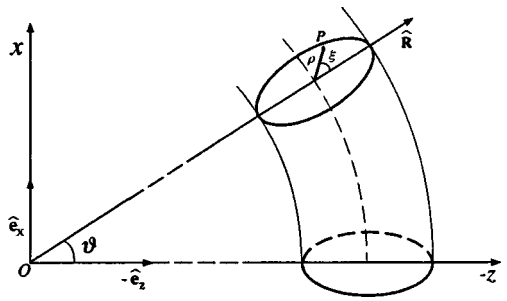

FIG. 3. Arc 1 of Fig. 1 with an enlarged cross section of the wire seen in perspective. The origin of the Cartesian coordinates is at the center O of the semicircular axis of arc 1. We have used polar coordinates ρ and ξ in each cross section, the angle ξ starting from $\mathbf{R}$.

$$\mathbf{F}=\int\int\int_1 d^3r\,\mathbf{j}(\mathbf{r})\times\mathbf{B}(\mathbf{r}), \tag{5}$$

with $\mathbf{B}(\mathbf{r})$ given by Eq. (4).

Because of symmetry, the resultant force on the mobile part of the circuit is parallel to the x axis, so Eq. (5) implies that the active sections are those that have components perpendicular to the x axis, i.e., arc 1 (see Fig. 1) and the two bent sections immersed in the mercury and parallel to the y axis (see details in Fig. 5 of Appendix A). The magnetic field at the position of arc 1 is due to all of the circuit including arc 1 itself. The force $\mathbf{F}_{\text{rest}}$ due to the rest of the circuit (excluding 1 itself) is easily calculated because we may approximate the real conductors by wires of infinitesimal cross sections. Consequently, Eqs. (4) and (5) reduce, if I_0 is the constant current flowing in the circuit, to

$$\mathbf{F}_{\text{rest}}=\frac{\mu_0 I_0^2}{4\pi}\int_1 d\mathbf{r}\times\int_{2+3+4+5+6} d\mathbf{r}'\times\frac{\mathbf{r}-\mathbf{r}'}{|\mathbf{r}-\mathbf{r}'|^3}. \tag{6}$$

It is convenient to separate the circuit into two parts, symmetric with respect to the x axis so that the contribution to the force on arc 1 and due to section 2 is equal to that of section 3, the contribution due to 6 is equal to that of 5, and the contributions of the two half sections 4 (one from $z=-R$ to $z=0$ and the other from $z=0$ to $z=R$) are equal. Setting

$$l'=l/R,\quad h'=h/R \tag{7}$$

and denoting by ϑ the angle between the radius vector $\mathbf{R}$ of arc 1 (see Fig. 1) and $-\hat{\mathbf{e}}_z$ (where $\hat{\mathbf{e}}_z$ is the unit vector of the z axis and $\hat{\mathbf{e}}_x$ and $\hat{\mathbf{e}}_y$ denote the unit vectors of the x and y axes, respectively), we obtain from Eq. (6) for the x component (which is the only one different from zero because of the axial symmetry around the x axis), after performing analytically the second integral,

$$F_{\rm rest}=\frac{\mu_0 I_0^2\sqrt{2}}{4\pi}\int_0^{\pi} d\vartheta\ \sin\vartheta\left\{\left[\frac{h'+l'+\sin\vartheta}{(1-\cos\vartheta)[(h'+l')^2/2+(h'+l')\sin\vartheta+(1-\cos\vartheta)]^{1/2}}-\frac{\sin\vartheta}{(1-\cos\vartheta)^{3/2}}\right]\right.$$

$$\left.+\frac{1}{\sin\vartheta+h'+l'}\left[\frac{\cos\vartheta}{[1/2+(h'+l')\sin\vartheta+(h'+l')^2/2]^{1/2}}+\frac{1-\cos\vartheta}{[(1-\cos\vartheta)+(h'+l')\sin\vartheta+(h'+l')^2/2]^{1/2}}\right]\right\}, \quad (8)$$

where the terms inside the two large square brackets correspond to the force on 1 due to sections 2, 6, 5, and 3, and section 4, respectively, of Fig. 1.

Now we have to calculate the force acting on arc 1 due to 1 itself. The corresponding magnetic field diverges logarithmically as the diameter of the conductor becomes infinitesimal. It is therefore essential to use a conductor of radius a. Consequently, R is the radius of the axis of the semicircular arc 1. Supposing that the current density $\mathbf{j}$ is uniform and parallel to the unit vector $\hat{\boldsymbol{\vartheta}}$ tangent to the arc passing through the considered point, it is $\mathbf{j}=\hat{\boldsymbol{\vartheta}}\, I_0/\pi a^2$. Consequently, the force on 1 (and due to 1 itself) is given by the sixfold integral obtainable by Eqs. (4) and (5),

$$\mathbf{F}_1=\frac{\mu_0}{4\pi}\left(\frac{I_0}{\pi a^2}\right)^2 \times\int\int\int_1 d^3r\int\int\int_1 d^3r'\,\frac{\hat{\boldsymbol{\vartheta}}\times[\hat{\boldsymbol{\vartheta}}'\times(\mathbf{r}-\mathbf{r}')]}{|\mathbf{r}-\mathbf{r}'|^3}. \quad (9)$$

To calculate this integral it is convenient to consider cross sections of the semicircular wire 1, i.e., circles obtained by intersecting the wire by planes containing $\mathbf{R}$ and perpendicular to the wire axis. We denote by ρ the distance of a generic point P (inside the circular cross section) from the wire axis and by ξ the angle between $\mathbf{R}$ and $\boldsymbol{\rho}$. Choosing the coordinate axes, as shown in Fig. 3, the radius $\mathbf{r}$ of a generic point is $\mathbf{r}=\mathbf{R}+\boldsymbol{\rho}$. Consequently, introducing the dimensionless quantity $s=\rho/R$, the coordinates of P are

$$x=R(1+s\ \cos\xi)\sin\vartheta,$$

$$y=-Rs\ \sin\xi, \quad (10)$$

$$z=-R(1+s\ \cos\xi)\cos\vartheta.$$

The Jacobian of the transformation from x,y,z to s,ξ,ϑ is $R^3 s(1+s\ \cos\xi)$. Then we obtain from Eq. (9) for the component of the force in the x direction

$$F_1=\frac{\mu_0}{4\pi}\left(\frac{I_0}{\pi a^2}\right)^2 R^4\int_0^{a/R} s\ ds\int_0^{a/R} s'ds'\int_0^{2\pi} d\xi\int_0^{2\pi} d\xi'\int_0^{\pi} d\vartheta\int_0^{\pi} d\vartheta'$$

$$\times\{(1+s\ \cos\xi)(1+s'\cos\xi')\sin\vartheta[(1+s'\cos\xi')-(1+s\ \cos\xi)\cos(\vartheta-\vartheta')]\}$$

$$\times\{2+s^2+s'^2+2(s\ \cos\xi+s'\cos\xi')-2ss'\sin\xi\sin\xi'-2(1+s\ \cos\xi)(1+s'\cos\xi')\cos(\vartheta-\vartheta')\}^{-3/2}. \quad (11)$$

Since the integrand contains an integrable divergence, the numerical calculation of this integral is very delicate and Appendix B is dedicated to it.

The results for the $\mathcal{S}$ and $\mathcal{L}$ configurations are given, respectively, by

$$F_{\rm rest\mathcal{S}}+F_1=\frac{\mu_0\ I_0^2}{4\pi}(1.4937+8.8015)=10.295\frac{\mu_0 I_0^2}{4\pi},$$

$$F_{\rm rest\mathcal{L}}+F_1=\frac{\mu_0\ I_0^2}{4\pi}(1.2704+8.8015)=10.072\frac{\mu_0 I_0^2}{4\pi}. \quad (12)$$

We see that the two theoretical results in Eq. (12) differ very little from each other, contrary to Pappas's [2] claim. Actually, Pappas supports the Ampère law as leading to results different from those obtainable by Grassmann's law [coming from the two Laplace's laws (4) and (5)]. Pappas claims that the Ampère law (which satisfies the action and reaction principle) implies a longitudinal action between the wire sections 6 and 2 (and between 5 and 3) that is larger than the forces on the rest of the circuit. This stronger force would be absent in the short configuration. On the contrary, the use of the Laplace laws (4) and (5) makes it intuitive that the only useful force is that acting on arc 1. Moreover, some of us [1] have shown that both the Grassmann and Ampère laws lead to the same result even if applied to the force on a part of a closed circuit. In any case, to give Pappas [2] a direct, experimental answer, we have used the two configurations (short and long).

The x component of the force on the two vertical sections V (see Fig. 5) immersed in the mercury has been calculated in Appendix A and turns out to be given by

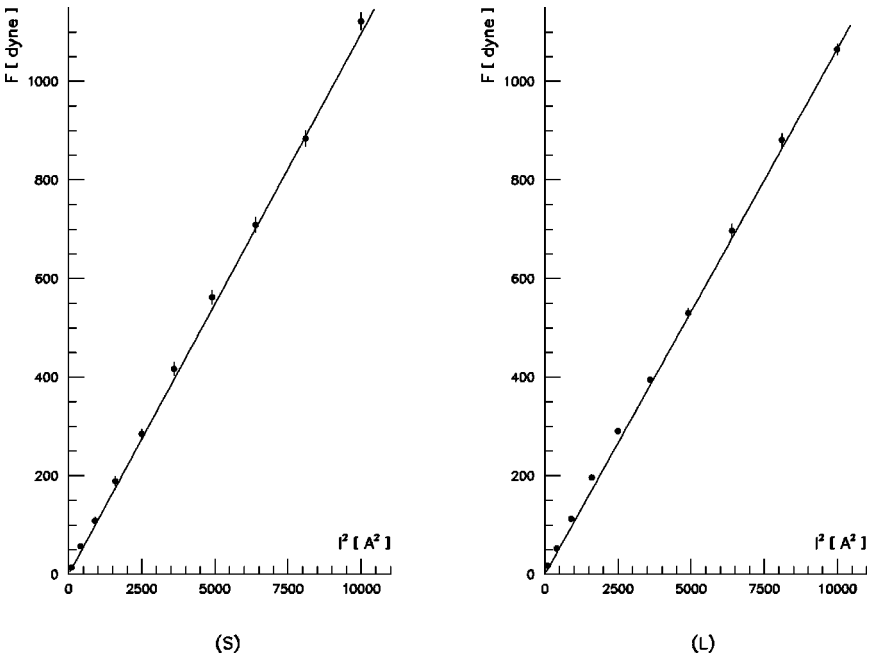

FIG. 4. Comparison between theoretical calculations (solid line) and experimental data (dots with error bars) for the force F on the mobile part when the current I_0 flows in the circuit. The results are relevant to (a) the short configuration and (b) the long configuration.

$$2F_{V\mathcal{S}}=0.6759(1\pm0.08)\frac{\mu_0 I_0^2}{4\pi},$$
$$2F_{V\mathcal{L}}=0.5839(1\pm0.08)\frac{\mu_0 I_0^2}{4\pi} \tag{13}$$

roughly 0.06 times the force on the mobile part of the circuit. We see that $2F_V$ is not negligible and has to be taken into account even in our configuration, which strongly reduces these forces with respect to Phipps's arrangement [3]. The total force turns out to be

$$F_{\mathcal{S}}=F_{\text{rest }\mathcal{S}}+F_1+2F_{V\mathcal{S}}=0.1097(1\pm0.006)I_0^2 \text{ dyn} \tag{14}$$

in the $\mathcal{S}$ configuration and

$$F_{\mathcal{L}}=F_{\text{rest }\mathcal{L}}+F_1+2F_{V\mathcal{L}}=0.1066(1\pm0.005)I_0^2 \text{ dyn} \tag{15}$$

in the $\mathcal{L}$ configuration, where I_0 is measured in amperes. The uncertainties in the theoretical calculations are mainly due to the approximations used in Appendix A to calculate the two forces F_V. The theoretical results are represented by the solid lines of Fig. 4(a) (short) and Fig. 4(b) (long).

IV. EXPERIMENTAL MEASUREMENTS

One of the causes of error is due to the action of the magnetic field **B** of the Earth. Fortunately, the corresponding force is proportional to I_0, so it changes sign when the direction of the current is reversed. It is apparent that the average value of this force is zero for two measurements made with the same value of I_0 but of opposite directions (I_0 and $-I_0$). On the other hand, the self-forces generated by the system depend on I_0^2 and are independent of the sign of I_0. Thus, if for a fixed, absolute value of I_0 the current is made to flow in one direction and then in the opposite direction, the resultant average is unaffected by the magnetic field of the Earth.

Another cause of error is due to the friction force on the two electrodes V partially immersed in the mercury (see Figs. 2 and 5) and caused by the surface tension of the mercury surface. For small values of the current I_0 this friction force can be one order of magnitude larger than the electrodynamical force. It has been necessary therefore to displace forcedly the mobile part by rotating the head of the torsion balance. Any displacement was the minimum necessary to trigger the forward impulse counter (whose sensor is a photodiode). Denote by $\mathbf{F}_f$ the forward force to produce the displacement. $\mathbf{F}_f$ is opposite the sum of the electrodynamical force $\mathbf{F}_{\text{ed}}$ and the forward friction force $\mathbf{F}_{\text{friction }f}$, i.e., $\mathbf{F}_f=-(\mathbf{F}_{\text{ed }f}+\mathbf{F}_{\text{friction }f})$. Then an opposite displacement is produced again by oppositely rotating the head of the torsion balance. Denote by $\mathbf{F}_b$ the corresponding backward force,

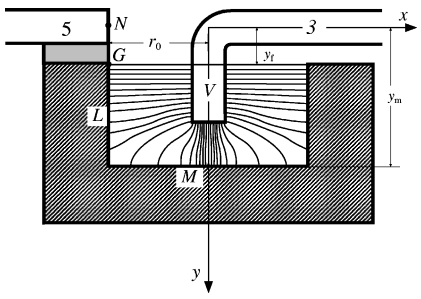

FIG. 5. Cross section of the mercury trough M_1 of Figs. 1 and 2, connected to the conductor 5 in the long configuration. The electrode V is partially immersed in the mercury and is the end of the conductor 3 of Figs. 1 and 2. We denote by L the internal lateral wall and by M the internal bottom of M_1. Moreover, N is the end center of conductor 5 and G is the intersection of a vertical axis (parallel to y) passing through N with the mercury surface whose ordinate is y_f. The ordinate of M is y_m. The shown flux lines of $\mathbf{j}=\sigma_m\mathbf{E}$ have axial symmetry because the conductivity σ_m of the mercury is much less than the conductivity σ_b of the bronze in the trough.

which can be written as $\mathbf{F}_b = -(\mathbf{F}_{\text{ed }b} + \mathbf{F}_{\text{friction }b})$. Notice that $\mathbf{F}_{\text{ed }f} \neq \mathbf{F}_{\text{ed }b}$ because the two electrodynamical forces are relevant to two different positions. If $\mathbf{F}_{\text{friction }f} \simeq -\mathbf{F}_{\text{friction }f}$, adding the above expressions gives for the electrodynamical or net force, when $|\mathbf{F}_{\text{ed}}| > |\mathbf{F}_{\text{friction}}|$,

$$\langle \mathbf{F}_{\text{ed}} \rangle = \frac{1}{2}(\mathbf{F}_{\text{ed }f} + \mathbf{F}_{\text{ed }b}) = -\frac{1}{2}(\mathbf{F}_b + \mathbf{F}_f). \tag{16}$$

To take the average of backward and forward forces as the ''average'' electrodynamical force implies a 0.3% error since the force on the conductor V of the mercury trough is not linear with the displacement but roughly inversely proportional to the distance from NGL of Fig. 5. Moreover, an uncertainty of 2 mm of the exact positioning of V implies an uncertainty of 8% in the force on V. Since $2F_V$ is $\simeq$ 6% of the total force, the mentioned uncertainty implies $\simeq \pm 0.4\%$ uncertainty for the total force.

Possible asymmetries in the friction forces, i.e., if $\mathbf{F}_{\text{friction }f}$ differs appreciably from $-\mathbf{F}_{\text{friction }b}$, bring about asymmetries in the experimental values leading to an interpolating curve for F that does not vanish when the current I_0 vanishes. When $|\mathbf{F}_{\text{ed}}| < |\mathbf{F}_{\text{friction}}|$ the external force $\mathbf{F}_b$ is parallel to $\mathbf{F}_{\text{ed}}$ so the latter is given by

$$\mathbf{F}_{\text{ed}} = \frac{1}{2}(\mathbf{F}_f - \mathbf{F}_b). \tag{17}$$

It was impossible to obtain reliable data without this averaging procedure. The friction force due to the surface layer of mercury increased with time t and in particular after the temperature of the mercury increased around 50 °C when operating at high current intensities ($\simeq$100 A). Actually, a high temperature favored the formation of a small amount of amalgam while the dust depositing on the mercury surface increased with time, thus forming an almost elastic membrane. We therefore purified the mercury by means of a filter after any group of measurements.

Another improvement has been achieved by using a second torsion balance B_2 (see Fig. 2) that exerts a traction somewhat larger than the friction force. B_2 eliminates the mechanical plays and also allows one to use Eq. (16) only. In fact, balance B_1 has to exert a force always opposite $\mathbf{F}_{\text{ed}}$ even when $|\mathbf{F}_{\text{ed}}| < |\mathbf{F}_{\text{friction}}|$ and there is no longer the necessity to use Eq. (17).

We have collected 6000 reliable experimental data of which 2000 were needed to obtain the equilibrium point in the absence of the current I_0. The 4000 useful values have been divided into 20 different values for the current intensity I_0. For each of the 200 values relative to the same value of I_0 we have made different groups of measurements, which are reported in Fig. 4(a) for the $\mathcal{S}$ configuration and in Fig. 4(b) for the $\mathcal{L}$ configuration as a function of I_0^2 so as to have straight interpolating lines (as required by theory). Actually, the best interpolating straight lines according to the least-squares method do not pass through the origin, showing a clear error due to some bias (for instance, the surface tension of the mercury trough for an inexact symmetry between the two positions, forward and backward, as explained in Sec. II). Since we are interested in the slopes of the two interpolating straight lines, standard error analysis gives for it an error of $\simeq$ 0.8%, which increases to 1% if we impose, as we should, that the straight lines pass through the origin. This is what we have done in Fig. 4. Standard error analysis has been applied to the data to obtain the standard deviation. The average value of the experimental force F_{ex} and its standard deviation turn out to be given by

$$F_{\text{ex}\,\mathcal{S}} = 0.1107(1 \pm 0.01) I_0^2 \ \text{dyn} \tag{18}$$

in the $\mathcal{S}$ configuration and by

$$F_{\text{ex}\,\mathcal{L}} = 0.1077(1 \pm 0.01) I_0^2 \ \text{dyn} \tag{19}$$

in the $\mathcal{L}$ configuration. Comparing the experimental results (18) and (19) with the theoretical results (14) and (15), we see that they agree to within experimental errors and theoretical approximations [see Fig. 4(a) and Fig. 4(b)]. Consequently, our experimental results contradict those of Pappas [2] and confirm the standard theory.

V. CONCLUSIONS

Our ''old-fashioned'' experiment of classical electrodynamics shows in a definitive way that there is agreement between experimental data and the theoretical values calculated by standard theory. ''Old fashioned'' is with regard to the kind of experiment, but not the experimental apparatus and the computers necessary to perform the sixfold integral.

The agreement found (inside the experimental and the numerical computations) allows us to disprove all the papers [4] claiming the standard theory to be wrong and that there are no direct, recent, dedicated experiments. In another paper [5], special mention is made of a recent work of Assis [6], who claims to derive gravitation from Weber's force law (another elementary law).

ACKNOWLEDGMENTS

We wish to thank the CNR (Italy) and the CDCHT ULA, Mèrida, Venezuela, for sponsoring this research.

APPENDIX A

1. The mercury trough and generalities for the calculation of the force on the section V immersed in the mercury

After many attempts we have found that a convenient, practical arrangement for the electrical connections is that shown in Fig. 5, where we consider the mercury trough M_1 (see Fig. 1). We must calculate the force $\mathbf{F}_V$ on the vertical section V belonging to the mobile part of the circuit and partially immersed in the mercury. We take the y axis as symmetric to V and the x axis as symmetric to the horizontal wire 3. The contributions to $\mathbf{F}_V$ antiparallel to x come from the wires 3 and 5 in the long configuration and only from 3 in the short version. It is $|\mathbf{F}_{V5}| \ll |\mathbf{F}_{V3}|$ with $F_{V3} < 0$. The contributions parallel to the x axis are due to the bottom M of the mercury trough (denoted by F_{V_M}), the lateral wall L (denoted by F_{V_L}), and the current connecting the center N of the ending cross section of 5 with the point G at the free surface of the mercury (denoted by $F_{V_{NG}}$).

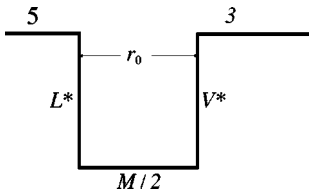

FIG. 6. Circuit, made of filiform wires, roughly approximating the mercury trough of Fig. 5, in particular of 5, NGL, M, V, and 3.

The currents in 3, 5, and NG may be considered as wirelike and having the full value I_0. The contribution of the opposite arm 2 (parallel to 3 and with $z=2R$) is less than $10^{-3}F_3$ and we neglect it. The calculation of $\mathbf{F}_{V_L}+\mathbf{F}_{V_M}$ is extremely difficult to perform in a rigorous way because the current density $\mathbf{j}$ inside the mercury must satisfy the continuity equation $\boldsymbol{\nabla}\cdot\mathbf{j}=0$ (in steady-state conditions) and is related to the electric field $\mathbf{E}$ by $\mathbf{j}=\sigma_m\mathbf{E}$, where σ_m is the conductivity of the mercury. In turn, $\mathbf{E}$ is related to the scalar potential φ by $\mathbf{E}=-\boldsymbol{\nabla}\varphi$ and φ satisfies the Laplace equation $\nabla^2\varphi=0$.

A second, more difficult problem is that we cannot obtain the force $\mathbf{F}_V$ by simply calculating the Lorentz force on the conductor V. Actually, the Lorentz force acts also on the current distributed in the mercury so that the electrons are slightly displaced from their ions and a very small electric charge appears on the surface of the mercury, on the lateral wall L, and on V. Consequently, an electrostatic force comparable to the magnetic one acts on V. Because of this, we first approximate the mercury trough by a simple circuit made of filiform wires, as shown in next section.

2. An equivalent circuit made of filiform wires

As a first approximation we present a schematic of the mercury trough by the filiform (i.e., with zero cross section) circuit shown in Fig. 6. The wires 5 and 3 (now represented only by their axes) remain the same, while the conductor V is prolonged up to the bottom $M/2$, where /2 denotes that it has a length equal to half the diameter of the mercury trough. The lengthening of V^* up to $M/2$ is necessary in order to take into account the current distribution in the mercury on which the Lorentz force acts. This force is transmitted to V in Fig. 5 and to V^* in Fig. 6 via the electrostatic force (due to the displacement of the charges in the mercury). The length of L^* (equal to that of V^*) is less than the y_m of Fig. 5 because the flux lines of $\mathbf{j}$ are distributed in the mercury starting from its surface up to the bottom M. Precisely, with reference to Fig. 5, we leave unaltered NG and reduce by a fraction $\simeq 0.5$ the distance of G from M. Consequently, the new y_m^* is

$$y_m^*=y_f+0.5(y_m-y_f). \tag{A1}$$

The forces on V^* and due to 5 and L^* are calculated by considering V^* as a straight segment connecting $M/2$ to 3. If the same procedure is adopted to calculate the forces on V^* due to 3 and $M/2$ we would obtain two logarithmic divergences that are equal and opposite. We therefore eliminate two short connections of V^* (connecting it with $M/2$ and 3) when we calculate the actions of 3 and $M/2$ on V^*.

We then apply Eq. (6) of the main text, which in our case becomes

$$\begin{aligned}\left(\frac{\mu_0 I_0^2}{4\pi}\right)^{-1} F_{V^*} &= \int_{V^*} d\mathbf{r}\times\int_{5+3+M/2+L^*} d\mathbf{r}'\times\frac{\mathbf{r}-\mathbf{r}'}{|\mathbf{r}-\mathbf{r}'|^3}\cdot\hat{\mathbf{e}}_x \\ &= -\int_0^{y_m^*} dy\int_{-l}^{-r_0} dx\,\frac{y}{(x^2+y^2)^{3/2}} \\ &\quad -\int_{R_V}^{y_m^*-R_V} dy\int_0^h dx\,\frac{y}{(x^2+y^2)^{3/2}} \\ &\quad +\int_{R_V}^{y_m^*-R_V} dy\int_{-r_0}^0 dx\,\frac{y_m^*-y}{[x^2+(y_m^*-y)^2]^{3/2}} \\ &\quad +\int_0^{y_m^*} dy\int_0^h dy'\,\frac{r_0}{[r_0^2+(y-y')^2]^{3/2}},\end{aligned} \tag{A2}$$

where r_0, h are given by Eqs. (2) and (3), y_m^* is given by Eq. (A1), $R_V=1.5a$ [with $a=0.25$ cm given by Eq. (3)], $l=61.62$ cm in the $\mathcal{L}$ configuration, and $l=r_0$ in the $\mathcal{S}$ configuration. The results for the $\mathcal{S}$ and $\mathcal{L}$ configurations are given, respectively, by

$$\begin{aligned}F_{V^*\mathcal{S}} &= 0.3942\frac{\mu_0 I_0^2}{4\pi} \quad \text{for } \mathcal{S}, \\ F_{V^*\mathcal{L}} &= 0.3118\frac{\mu_0 I_0^2}{4\pi} \quad \text{for } \mathcal{L}.\end{aligned} \tag{A3}$$

3. Calculation of the force on V in the real situation with distributed current

Let us now return to the real configuration shown in Fig. 5. The results of the preceding section show that the joint contribution of the two conductors V (immersed in the two mercury troughs) is $\simeq$ 6% of the total force. It is therefore sufficient to calculate F_V with a 10% approximation to have a 0.6% approximation for the total force whose experimental value has an uncertainty of 1%. Hence it is useless to face the extremely difficult problem of looking for an exact value. Moreover, a change of more than 20% in the distribution of the current in the mercury produces a variation of F_V less than 5%. Consequently, we proceed in an approximate way that guarantees a value for F_V within a 10% approximation.

The difficulty that comes from the boundary conditions may be simplified greatly if the trough is considered as equipotential. This simplification is justified since $\sigma_m=0.033\sigma_b$, where σ_b is the conductivity of the bronze constituting the trough. In this case the magnetic field $\mathbf{B}$ due to the current flowing in the mercury vanishes because of the axial symmetry of the distribution of $\mathbf{j}$. Consequently, the force on V due to this $\mathbf{j}$ vanishes. It is also possible to draw with a good approximation the distributions of the flux lines for both $\mathbf{j}$ and $\mathbf{E}$, as shown in Fig. 5. The distribution of the current density j (per unit surface) on the lateral wall L is fairly well approximated by

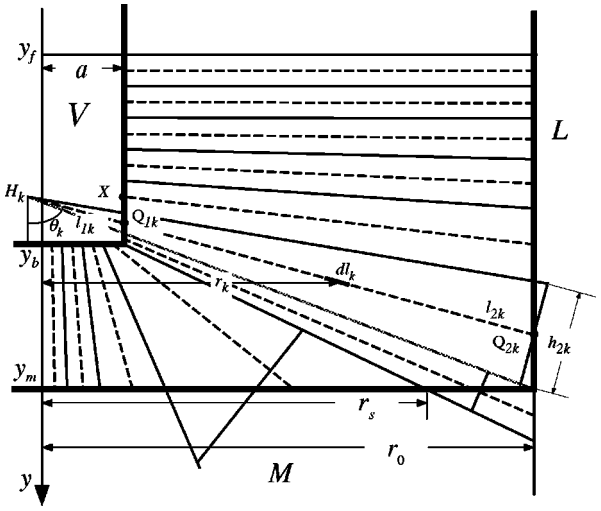

FIG. 7. Cross section of half M_1 with traces of flux tubes of the current density **j** flowing in the mercury, schematized as straight lines. Their axes are shown by dashed straight lines. r_0 is the radius of the internal wall L and r_s the intersection with M of the flux line issuing from the corner of the cross section of V.

$$j = j_0 \cos\left[\frac{\pi(y-y_f)}{2(y_m-y_f)}\right] = j_0 \cos T. \tag{A4}$$

The constant j_0 will be obtained from the current I_L flowing into the mercury from the lateral wall L. To find the distribution of j on the internal base M of the mercury trough we notice that some flux lines issuing from the lateral wall of V end on an annular strip between $r_s \simeq 0.828 r_0$ and r_0, the latter being the maximum radius of M (see Fig. 7). This modifies the known behavior of the flux lines due to a disk facing an indefinite plane. Moreover, j must vanish in the connection between L and M, i.e., for $r = r_0$. By these criteria the current density on M (with $0 < r < r_0$) is approximated by

$$j = j_0^* \left[0.321 + \cos\left(\frac{\pi r}{2 r_s}\right)\right]^2. \tag{A5}$$

The constant j_0^* will be obtained from the current I_M flowing into the mercury from M (see Fig. 5). The currents I_L and I_M are obtained by two conditions: (i) $I_L + I_M = I_0$, where I_0 is the total current flowing in the circuit, and (ii) $I_L / I_M = R_{V_M} / R_{V_L}$, where R_{V_L} is the resistance between the electrode V and L and R_{V_M} is the resistance between the electrode V and M.

To obtain a good approximation for the values of R_{V_L} and R_{V_M} we have divided the flux tubes starting from the lateral wall V_L of the central conductor V into six parts and those starting from the bottom b of V into four parts, as shown in Fig. 7. Of the six parts starting from V_L, five end on L, while the sixth part ends partially on L (roughly $\simeq 2/3$) and partially on M (roughly $\simeq 1/3$). The four parts starting from V_b end on M. The spacing of the traces of the flux tubes on the xy plane is inversely proportional to the current densities given by Eq. (A4) for the lateral wall L and by Eq. (A5) for the bottom M. For simplification we have taken straight flux lines for the current. Then we get

$$\frac{1}{R_{V_L}} = \sum_{k=1}^{6} \frac{1}{R_{L_k}} \tag{A6}$$

and

$$\frac{1}{R_{V_M}} = \sum_{k=1}^{5} \frac{1}{R_{M_k}}, \tag{A7}$$

where the sixth contribution to Eq. (A6) and the fifth contribution to Eq. (A7) are roughly due to 2/3 and 1/3, respectively, of the sixth flux tube starting from V_L.

We write as an example the explicit calculations for a generic kth resistance R_k of the kth gap between truncated cones whose traces on the xy plane are shown in Fig. 7:

$$R_k = \frac{1}{\sigma_m} \int_{l_{1k}}^{l_{2k}} \frac{dl_k}{S_k(l_k)}, \tag{A8}$$

where σ_m is the mercury conductivity, dl_k an element of the axis of the kth flux tube trace, and $S_k(l_k)$ the variable cross section of the kth flux tube. The limits of integration are obtained as follows. Prolong the traces of the kth flux tube until they cross at a point H_k shown in Fig. 7 for $k = 6$. Then l_{1k} is the length of the segment $H_k Q_{1k}$ of Fig. 7, i.e., the distance from H_k of the intersection of the kth axis with the external wall of the conductor V, while l_{2k} is the segment $H_k Q_{2k}$, i.e., the distance from H_k of the intersection of the kth axis with the internal wall of the mercury trough.

If $h_k(l_k)$ is the transversal thickness of the kth flux tube trace and h_{2k} its final value (where the flux tube intersects the mercury trough), we have $h_k / h_{2k} = l_k / l_{2k}$. If θ_k is the angle between y and the axis of the kth flux tube and x_k is the abscissa of H_k (negative in the case of the sixth flux tube), the distance from y of the generic point of the flux tube axis is $x_k + l_k \sin\theta_k$. Consequently, the cross section of the kth flux tube is given by

$$S_k(l_k) = h_k 2\pi(x_k + l_k \sin\theta_k) = 2\pi h_{2k}(l_k / l_{2k})(x_k + l_k \sin\theta_k). \tag{A9}$$

The integral (A8) becomes therefore

$$R_k = \frac{l_{2k}}{2\pi\sigma_m h_{2k}} \ln\left[\frac{l_{2k}}{l_{1k}} \frac{x_k + l_{2k}\sin\theta_k}{x_k + l_{1k}\sin\theta_k}\right]. \tag{A10}$$

From Eqs. (A6), (A7), and (A10) and the values

$$a = 0.25 \text{ cm}, \quad r_s = 1.258\,32 \text{ cm}, \quad r_0 = 1.52 \text{ cm},$$
$$y_f = 0.5625 \text{ cm}, \quad y_b = 1.15 \text{ cm}, \quad y_m = 1.6 \text{ cm}, \tag{A11}$$

we obtain

$$R_{V_L} = \frac{2.666}{2\pi\sigma_m}, \quad R_{V_M} = \frac{4.941}{2\pi\sigma_m}, \tag{A12}$$

so

$$\frac{I_M}{I_L} = \frac{R_{V_L}}{R_{V_M}} = 0.539\,57. \tag{A13}$$

Since $I_0 = I_M + I_L$ we have finally

$$I_L = 0.6495 I_0, \quad I_M = 0.3505 I_0. \tag{A14}$$

Now from

$$I_L = j_0 2\pi r_0 \int_{y_f}^{y_m} dy \ \cos T = j_0 4 r_0 (y_m - y_f) \tag{A15}$$

we obtain, with the use of Eq. (A14),

$$j_0 = \frac{0.6495 I_0}{4 r_0 (y_m - y_f)} = 0.102\,96\ I_0, \tag{A16}$$

where j_0 is measured in Am^{-2}. Similarly, from

$$I_M = j_0^* 2\pi \int_0^{r_0} dr\ r\left[0.321 + \cos\left(\frac{\pi r}{2 r_s}\right)\right]^2$$

$$= j_0^* \frac{8}{\pi} r_s^2 \left\{ \frac{1}{2} (0.321 s)^2 + 0.642[\cos(s) + s\ \sin(s) - 1] + \left[\left(\frac{s}{2}\right)^2 + \frac{s}{4}\sin(2s) + \frac{1}{8}\cos(2s) - \frac{1}{8}\right]\right\}, \tag{A17}$$

where $s = \pi r_0 / 2 r_s$, we get, from Eqs. (A14) and (A17),

$$j_0^* = 0.098\,92 I_0. \tag{A18}$$

Having obtained the distribution of the current densities issuing from L and M it is possible to get the current I in the central conductor V, taking, with a good approximation, the current densities j_{Vb} and j_{V_L} on the base and the lateral wall, respectively, of V, as uniform. Denote by $I_{L+M\to V_L}$ the current ending on the lateral wall of V and starting partially from the lateral wall L of the trough and partially from the bottom M of the trough. Denote by $I_{M\to Vb}$ the current starting from the large central part of the bottom M of the trough and ending on the base b of V. We thus have

$$I_{L+M\to V_L} = I_L + \Delta I \tag{A19}$$

and

$$I_{M\to Vb} = I_M - \Delta I, \tag{A20}$$

where the contribution ΔI to the bottom M of the trough is given by the integral in Eq. (A17) where the lower limit is set equal to r_s. Inserting the values given by Eqs. (A11) and (A18) gives

$$\Delta I = 0.0072 I_0. \tag{A21}$$

We get from Eqs. (A14), (A19), (A20), and (A21)

$$I_{L+M\to V_L} = 0.6567 I_0, \quad I_{M\to Vb} = 0.3433 I_0. \tag{A22}$$

Consequently, the current I in V turns out to be given by

$$I = I_{M\to Vb} + \frac{y_b - y}{y_b - y_f} I_{L+M\to V_L} = \left(0.3433 + 0.6567 \frac{y_b - y}{y_b - y_f}\right) I_0. \tag{A23}$$

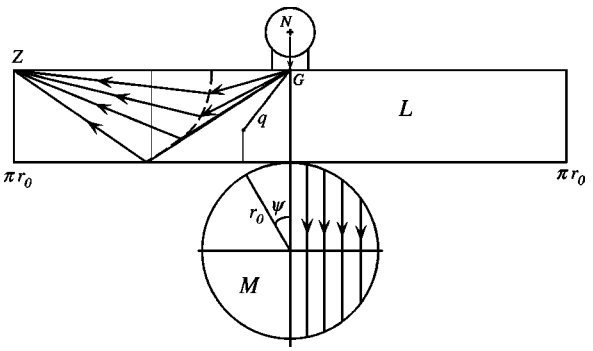

FIG. 8. Wall L of Figs. 5 and 7 has been expanded so as to be tangential to the internal bottom M at a point having coordinates $x = -r_0$ and $y = y_m$. Some flux lines (schematized by straight segments) of superficial current J flowing in the bronze are shown (J_L on L and J_M on M).

It is more difficult to evaluate the currents J_L and J_M per unit length on the lateral wall L and the bottom of the mercury M, respectively. It would be necessary to solve $\nabla^2 \varphi = 0$ with partially Dirichlet and Neumann conditions, taking into account the effective values of the conductivities. It is much easier to give approximated, sensible expressions that keep the error in the calculation of F_V to within 5%. The most important contribution to F_V is due to the J_L near G since, because of the current flowing in the mercury, J_L progressively decreases as we consider parts of L further and further from G and vanishes in Z (opposite G; see Figs. 5 and 8). With a very good approximation, J_L is radial in the part of L that starts from G and extends symmetrically from the plane p of symmetry containing the x and y axes, down to M (vertically) and, laterally, to a line $\psi = \psi(y)$ we determine later (see Fig. 8). Using as coordinates y and the distance q from G ($x = -r_0$, $y = y_f$), for $y > y_f$ we have the continuity equation

$$\frac{d(J_L q)}{dq} = -jq. \tag{A24}$$

The coordinates of a point on L are q and the angle ψ between the plane containing the y axis and passing through G and the plane passing through the y axis and the considered point. Let us integrate Eq. (A24), valid for $0 < \psi < \psi(y)$ and $y_f < y < y_m$, along the straight lines $y - y_f = m r_0 \psi$ (where m is the angular coefficient). For $q \to 0$ we must have $I_0 = J_L \pi q$ so that use of Eq. (A4) gives

$$J_L q - \frac{I_0}{\pi} = -\int_{y_f,\psi=0}^{y,\psi} j_0 \cos T [(r_0 d\psi)^2 + dy^2]^{1/2} \times [(r_0 \psi)^2 + (y - y_f)^2]^{1/2}. \tag{A25}$$

Since $d\psi = dy (m r_0)^{-1}$ and with T given by Eq. (A4) we get

$$J_L q - \frac{I_0}{\pi} = -j_0 \int_{y_f}^{y} dy (y - y_f)(1 + m^{-2}) \cos\left(\frac{\pi}{2} \frac{y - y_f}{y_m - y_f}\right), \quad 0 < \psi < \psi(y), \tag{A26}$$

whence

$$J_L=[(r_0\psi)^2+(y-y_f)^2]^{-1/2}\left\{\frac{I_0}{\pi}-\frac{j_0}{T^2}[(r_0\psi)^2+(y-y_f)^2]\times(T\sin T+\cos T-1)\right\},\qquad 0<\psi<\psi(y). \tag{A.27}$$

The y and the azimuthal components are given, respectively, by

$$J_{Ly}=J_L(y-y_f)/q,\quad J_{L\psi}=J_L r_0\psi/q, \tag{A28}$$

so in vector form we have

$$\mathbf{J}_L=J_L[(y'-y_f)\hat{\mathbf{e}}_y+r_0\psi(\hat{\mathbf{e}}_x\sin\psi-\hat{\mathbf{e}}_x\cos\psi)]/q, \tag{A29}$$

where $\hat{\mathbf{e}}_x,\hat{\mathbf{e}}_y,\hat{\mathbf{e}}_z$ are the unit vectors of the Cartesian axes and J_L is given by Eq. (A27).

The flux lines of the currents per unit lengths are plotted in Fig. 8 which shows the mercury trough expanded on the plane of the sheet, having ideally cut M along its periphery and L along the generatrix passing through Z (see Figs. 5 and 8). For $\psi>\psi(y)$ we have verified that straight, radial flux lines are still a good approximation provided they converge to the point at $y=y_f$ and $\psi=\pi$ (upper corner of the lateral wall). The current distribution J'_L [we add a prime to distinguish it from the J_L given by Eq. (A26)] is still given by Eq. (A27) without the first term, with a reverse sign of the second term, and $q'=[r_0^2(\pi-\psi)^2+(y-y_f)^2]^{1/2}$ instead of q, i.e.,

$$J'_L=j_0T^{-2}\{[(\pi-\psi)r_0]^2+(y-y_f)^2\}^{1/2}(T\sin T+\cos T-1),\qquad \psi>\psi(y). \tag{A30}$$

The y and ψ components are similar to those given by Eq. (A28), i.e.,

$$J'_{Ly}=-J'_L\frac{y-y_f}{q'},\quad J'_{L\psi}=J'_L\frac{r_0(\pi-\psi)}{q'}, \tag{A31}$$

or, in vector form,

$$\mathbf{J}'_L=J'_L[(y_f-y')\hat{\mathbf{e}}_y+r_0(\pi-\psi)(\hat{\mathbf{e}}_x\sin\psi-\hat{\mathbf{e}}_z\cos\psi)]/q', \tag{A32}$$

with J'_L given by Eq. (A30).

The line $\psi=\psi(y)$ is obtained by equating

$$J'_L(y,\psi)=J_L(y,\psi) \tag{A33}$$

and turns out to be given by

$$\psi(y)=0.772\,181y^2-0.982\,268y+1.139\,38. \tag{A34}$$

This line is shown by a dashed line in Fig. 8.

A good approximation for the current J_M per unit length flowing on the bottom M of the mercury trough is a pattern of straight flux lines (see Fig. 8). The values for $J_M(r_0,\psi)$ have to be equal to the corresponding ones of the lateral current for $y=y_m$, i.e.,

$$J_L(y_m,\psi)=J_M(r_0,\psi). \tag{A35}$$

The continuity equation on M is $\partial J_M/\partial x=-j$, which has to be integrated along the straight line $z=-r_0\sin\psi$ giving, with the use of Eq. (A5),

$$J_M(x,\psi)=J_M(r_0,\psi)-j_0^*\int_{-r_0\cos\psi}^{x}dx\left\{0.321+\cos\left[\frac{\pi}{2}(x^2+r_0^2\sin^2\psi)^{1/2}/r_s\right]\right\}^2. \tag{A36}$$

The reliability of this result is due to the check that for $x=r_0\cos\psi$ (the terminal of flux lines on M) Eq. (A35) is still satisfied to within 1% of the value at $x=-r_0\cos\psi$ (the beginning of the flux lines on M). Actually, the flux lines on L and M should be rounded so as to have continuous derivatives. However, the simplification shown in Fig. 8 is sufficient to guarantee an error less than 1% in small region of the walls and hence an error less than 0.1% for the force on V.

We have now all the elements to calculate the force on V. However, as already said in Secs. 1 and 2, the Lorentz forces on the current flowing on mercury are transmitted to V via the electrostatic forces due to the tiny displacement of the electrons with respect to their ions. An equivalent way to take into account this force is to calculate the whole force on the current flowing in V up to a V cross section intermediate between a first cross section where the **j** flux lines in the mercury begin to bend downward appreciably and the cross section where the issuing **j** lines reach the bottom M of the mercury trough. Then starting from this cross section, we consider a constant current along the y axis up to the bottom M. A point of the mentioned intermediate cross section is denoted by X of Fig. 8. Its ordinate is

$$y_X=1.0031\ \text{cm}. \tag{A37}$$

The current I flowing through cross section X is, as obtained from Eq. (A23) by setting $y=y_X$,

$$I_X=0.5075I_0. \tag{A38}$$

Then we keep $I=I_X$ from y_X to y_m. Summarizing, the effective current on which we must calculate the Lorentz force is

$$I=I_{V\text{eff}}=\begin{cases} I_0 & \text{for } 0\leqslant y<y_f \\ 0.3433I_0+0.6567\left(\dfrac{y_b-y}{y_b-y_f}\right)I_0 & \text{for } y_f\leqslant y<y_X \\ I_X & \text{for } y_X\leqslant y\leqslant y_m. \end{cases} \tag{A39}$$

At this point we can calculate the force on V in the $\mathcal{L}$ configuration due to wire 5, section NG, and the lateral wall L. Denoting by $\hat{\mathbf{e}}_x,\hat{\mathbf{e}}_y,\hat{\mathbf{e}}_z$ the unit vectors of the Cartesian axes we have for the x component of the force

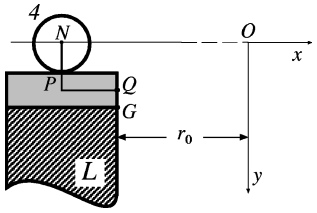

FIG. 9. Connection of wire 4 of Figs. 1 and 2 with the mercury trough for the $\mathcal{S}$ configuration. This detail replaces part 5, NG, and the beginning of L of Fig. 5 (which is relevant to the $\mathcal{L}$ configuration).

$$F_{V5}+F_{V_{NG}}+F_{V_L}=\hat{\mathbf{e}}_x\cdot\int_0^{y_m}dy\ I(-\hat{\mathbf{e}}_y)\times\mathbf{B}(y)$$
$$=-\int_0^{y_m}dy\ IB_z, \tag{A40}$$

where I is given by Eq. (A39) and B_z by

$$B_z=B_{z5}+B_{z_{NG}}+B_{z_L}$$
$$=\frac{\mu_0 I_0}{4\pi}\left\{\frac{1}{y}\left[\frac{l}{(l^2+y^2)^{1/2}}-\frac{r_0}{(r_0^2+y^2)^{1/2}}\right]\right.$$
$$+\frac{1}{r_0}\left[\frac{y_f-y}{[r_0^2+(y-y_f)^2]^{1/2}}+\frac{y}{(r_0^2+y^2)^{1/2}}\right]$$
$$+2r_0\int_{y_f}^{y_m}dy'\left[\int_0^{\psi(y')}d\psi\ \hat{\mathbf{e}}_z\cdot\mathbf{J}_L\times\frac{\mathbf{r}-\mathbf{r}'}{|\mathbf{r}-\mathbf{r}'|^3}\right.$$
$$\left.\left.+\int_{\psi(y')}^{\pi}d\psi\ \hat{\mathbf{e}}_z\cdot\mathbf{J}_L'\times\frac{\mathbf{r}-\mathbf{r}'}{|\mathbf{r}-\mathbf{r}'|^3}\right]\right\}, \tag{A41}$$

where $\mathbf{J}_L$ and $\mathbf{J}_L'$ are given by Eqs. (A29) and (A32), respectively, $\psi(y')$ is given by Eq. (A34), and

$$\mathbf{r}-\mathbf{r}'=r_0(\hat{\mathbf{e}}_x\cos\psi+\hat{\mathbf{e}}_z\sin\psi)+(y-y')\hat{\mathbf{e}}_y. \tag{A42}$$

Numerical calculations yield

$$F_{V5}+F_{V_{NG}}+F_{V_L}=0.4926\frac{\mu_0}{4\pi}I_0^2\ \text{ in }\ \mathcal{L}. \tag{A43}$$

In the $\mathcal{S}$ configuration, wire 5 is absent and wire 4 is electrically connected to the mercury trough as in Fig. 9. The average paths of the current are NP, PQ, and QG; from G the average path is as in the $\mathcal{L}$ configuration. Numerical calculations yield

$$F_{V_{NP}}+F_{V_{PQ}}+F_{V_{QG}}+F_{V_L}=0.5386\frac{\mu_0}{4\pi}I_0^2\ \text{ in }\ \mathcal{S}. \tag{A44}$$

In order to calculate the force on V due to wire 3 and the bottom M, we eliminate the first connection of V with 3 (with length $R_V=1.5\,a=0.375$ cm) and the last part of the (artificially) prolonged V near the bottom M (still R_V) since the effects of the two connections are equal and opposite and their exact calculations are very long. Actually, in our case the current I near M is smaller than I_0 whereas $I=I_0$ near conductor 3. However, the round connections of the **j** flux lines between those flowing inside V and those inside the mercury give a cumulative effect equal to and opposite that near 3. Consequently, we have for the x component of the force

$$F_{V_M}+F_{V3}=\hat{\mathbf{e}}_x\cdot\int_{R_V}^{y_m-R_V}dy\ I(-\hat{\mathbf{e}}_y)\times\mathbf{B}(y)$$
$$=-\int_{R_V}^{y_m-R_V}dy\ IB_z, \tag{A45}$$

where I is still given by Eq. (A39) and B_z by

$$B_z=B_{z_M}+B_{z3}$$
$$=\frac{\mu_0 I_0 r_0}{2\pi}\int_0^{\pi/2}d\psi\cos\psi\int_{-r_0\cos\psi}^{r_0\cos\psi}dx\ \hat{\mathbf{e}}_z\cdot\mathbf{J}_M\ \frac{\mathbf{r}-\mathbf{r}''}{|\mathbf{r}-\mathbf{r}''|^3}$$
$$+\frac{\mu_0 I_0}{4\pi y}\left[\frac{h}{(h^2+y^2)^{1/2}}-\frac{R_V}{(R_V^2+y^2)^{1/2}}\right], \tag{A46}$$

with $\mathbf{J}_M=J_M\hat{\mathbf{e}}_x$ and

$$\mathbf{r}-\mathbf{r}''=(y-y_m)\hat{\mathbf{e}}_y-x\hat{\mathbf{e}}_x+r_0\sin\psi\hat{\mathbf{e}}_z. \tag{A47}$$

Numerical calculations yield

$$F_{V_M}+F_{V_3}=-0.2007\frac{\mu_0}{4\pi}I_0^2. \tag{A48}$$

The force due to wire 4 on V is negligible since $\mathbf{B}_4$ is almost parallel to the y axis around V. The total force on V has therefore an x component given by

$$F_{V\mathcal{S}}=0.3379(1\pm0.08)\frac{\mu_0 I_0^2}{4\pi},$$
$$F_{V\mathcal{L}}=0.2919(1\pm0.08)\frac{\mu_0 I_0^2}{4\pi}. \tag{A49}$$

The values given by Eq. (A49) are somewhat less than, and in acceptable agreement with, the corresponding values (A3) obtained by the very rough approximation of a simple wire. Since we have two mercury troughs, the total force on the electrodes V is twice that given by Eq. (A49).

APPENDIX B

The integrand of Eq. (11) contains an integrable divergence, as is clear from Eq. (6). In fact, it diverges as $|\mathbf{r}-\mathbf{r}'|^{-2}$ for $\mathbf{r}'\to\mathbf{r}$ although, for any $\mathbf{r}$, the numerator has the third-order infinitesimal quantity d^3r' that makes the integral converge. This feature makes it difficult to evaluate numerically the integral with an accuracy of four significant figures. For instance, the usual best method, that of Gauss, cannot be applied since two subsequent zeros of Legendre polynomials can be highly asymmetric with respect to a point of divergence. The addition of a small quantity ϵ to the denominator of the integrand gives a small advantage since, if we fix five of the six variables of integration and vary the

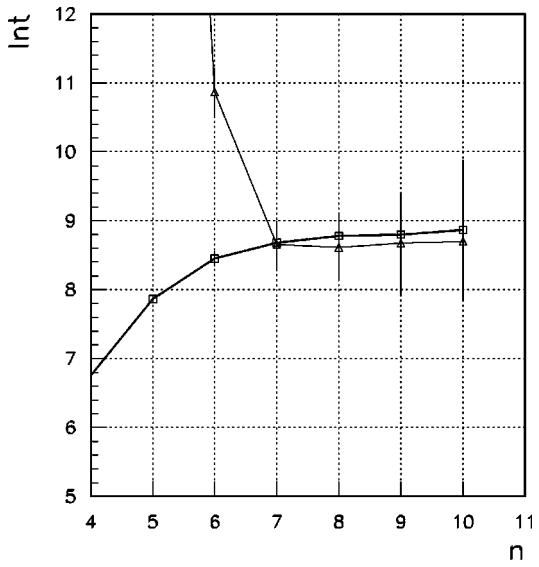

FIG. 10. The □ denote the numerical results and interpolating line b of the six-fold integral (11) obtained by a Monte Carlo method vs n, where n is the exponent of the smoothing term $\epsilon = 10^{-n}$ added to the denominator of Eq. (11), and the △ denote the numerical results and interpolating line d of the five-fold integral (B1) obtained by a Monte Carlo method.

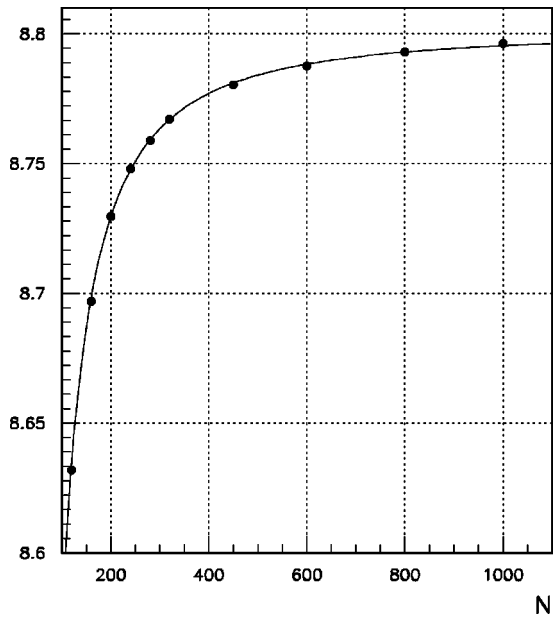

FIG. 11. Numerical results of the six-fold integral (11) vs the number N of points used for the variable ϑ (the variable ϑ', because of the axial symmetry of the circuit, requires $N/2$ points). The results are obtained by a regular division of the points, thus imitating the average behavior of the electrons.

sixth one, the divergence changes sign when we cross the point $\mathbf{r}'=\mathbf{r}$.

The quickest method to calculate multiple integrals is the Monte Carlo method. Adding $\epsilon=10^{-n}$ to the denominator of Eq. (11) and performing many calculations for each n, we have obtained the values shown by circles in Fig. 10. We see that there are strong fluctuations by changing the seed of the generated random numbers and the number N of points calculated. Strong fluctuations remain up to $N\simeq 2\times 10^9$. The interpolating line b is uncertain, so even the second significant figure is unreliable (see the caption of Fig. 10).

We have succeeded in performing an analytical calculation of the integral over s, thus reducing Eq. (11) to the five-fold integral

$$F_1=\frac{\mu_0}{4\pi}\left(\frac{I_0}{\pi a^2}\right)^2 R^4\int_0^{a/R} s'ds'\int_0^{2\pi}d\xi\int_0^{2\pi}d\xi' \times\int_0^{\pi}d\vartheta\int_0^{\pi}d\vartheta' s'\sin\vartheta(1+s'\cos\xi')\left\{-\frac{a_R^2 C}{\mathcal{R}+\epsilon} + \frac{C\cos\xi[Da_R(5F-6D^2)+F(2F-3D^2)]}{(F-D^2)\mathcal{R}+\epsilon} + \frac{(B\cos\xi-C)[a_R(F-2D^2)-FD]+B(F+Da_R)}{(F-D^2)\mathcal{R}+\epsilon} + \sqrt{F}\frac{C\cos\xi(2F-3D^2)-(B\cos\xi-C)D+B}{F-D^2+\epsilon} + (3DC\cos\xi+B\cos\xi-C)\ln\frac{|\mathcal{R}+a_R+D|+\epsilon}{|\sqrt{F}+D|+\epsilon}\right\}, \tag{B1}$$

where $a_R=a/R$ [with a and R given by Eq. (3)] and

$$B=(1+s'\cos\xi')-\cos(\vartheta-\vartheta'),$$

$$C=\cos\xi\cos(\vartheta-\vartheta'),$$

$$D=\cos\xi-s'\sin\xi\sin\xi'-(1+s'\cos\xi')\cos(\vartheta-\vartheta')\cos\xi, \tag{B2}$$

$$F=2+s'^2+2s'\cos\xi'-2(1+s'\cos\xi')\cos(\vartheta-\vartheta'),$$

$$\mathcal{R}=\sqrt{a_R^2+2Da_R+F}.$$

We have added the small quantity $\epsilon=10^{-n}$ in the denominator of Eq. (B1) as we have done for the six-fold integral. By the same procedure used for Eq. (11), we have obtained the values shown by triangles in Fig. 10 (still vs n). The accuracy of the interpolating line d is not better than the previous ones.

Finally, a good result for the integral has been obtained by imitating the average distribution of the electrons (producing the current in the considered wire) that are equally spaced. We have therefore divided each variable into equal parts and calculated the force on each point excluding the action of the considered point on itself. We then varied the number of divisions of each variable and verified that the results become insensitive to further increases after 30 divisions for ξ and ξ', 20 for s and s', while the convergence is very slow for ϑ and ϑ'. We have therefore drawn the plot, shown in Fig. 11, of the values of the integral versus N, which denotes the number of points of ϑ (we have divided the circuit into two parts exploiting its symmetry so that N' for ϑ' is equal

to $N/2$). There are no fluctuations and the curve interpolating the results is

$$\mathcal{J}=8.8015\left(1-\frac{21.742}{n^{3/2}-163.1729}\right), \tag{B3}$$

whose asymptotic value is 8.8015, so that

$$F_1=F_{1\text{self}}=8.8015\frac{\mu_0 I_0^2}{4\pi}. \tag{B4}$$

Since the contribution to the total force on the circuit is by far the largest one, its accuracy up to and including the fourth significant figure is necessary.

[1] G. Cavalleri, G. Spavieri, and G. Spinelli, Eur. J. Phys. **17**, 205 (1996).

[2] P. T. Pappas, Nuovo Cimento B **76**, 189 (1983).

[3] T. E. Phipps and T. E. Phipps, Jr., Phys. Lett. A **146**, 6 (1990); T. E. Phipps, Jr., in *Proceedings of the Conference on Physical Interpretation of Relativity Theory, London, 1990*, edited by M. C. Duffy (University of Sunderland, Sunderland, 1990), p. 435.

[4] See Refs. [2] and [3] and I. A. Robertson, Philos. Mag. **36**, 32 (1945); P. Moon and D. E. Spencer, J. Franklin Inst. **257**, 203 (1954); **257**, 305 (1954;); **257**, 369 (1954); H. Aspden, *ibid.* **287**, 179 (1969); **287**, 1997 (1969); IEEE Trans. Plasma Sci. **PS-14**, 282 (1986); Phys. Lett. A **120**, 80 (1987); P. Graneau, Nature (London) **295**, 311 (1982); Fortschr. Phys. **34**, 457 (1986); J. Appl. Phys. **62**, 3006 (1987); Wireles World **95**, 556 (1989); J. P. Wesley, Found. Phys. Lett. **3**, 443 (1990); **3**, 586 (1990).

[5] G. Cavalleri, G. Spavieri, and E. Tonni, Hadronic J. **21**, 459 (1998).

[6] A. K. T. Assis, Can. J. Phys. **70**, 330 (1992).